# **Solderability of Additively Manufactured Copper Surfaces**

# R. Wheeling\*, S. Williams, D. Tung, L. Juaregui, C. Profazi, M. Vieira, P. Vianco

Sandia National Laboratory
New Mexico, USA

\*Medtronic Inc. Minneapolis, MN, USA

#### **ABSTRACT**

As additive manufacturing technology for copper rapidly evolves, the likelihood for downstream joining like soldering and brazing exists. A solderability study was performed to assess process fundamentals over a variety of AM approaches. The solderability of 7 different copper (Cu) surface types were evaluated using the wetting balance technique: 4 Cu coatings (CP-007 and CP-008 conductive copper pastes, IMC-4118 conductive laser sinter paste, IMC-2501 copper ink), 2 laser processed Cu surfaces, and 1 bulk additively manufactured (AM) Cu coupon type. Laser processed surfaces were subjected to either circular or linear laser raster patterns. AM coupons were fabricated via a powder-bed laser process. In-situ force measurements were recorded while coupons were dipped into and removed from a 63Sn-37Pb (SnPb) or 96.4Sn-3.0Ag-0.6Cu (SAC305) solder bath, allowing contact angles and surface energies to be calculated. Meniscus height values were also measured. Surfaces were characterized before and after dipping via optical and electron microscopy. Results conclusively indicated that although all samples were intended to represent pure Cu, wettability was found to be strongly dependent on surface type with several samples exhibiting no wetting. Although the CP-007 paste performed the best of any non-traditional surface, all nontraditional surfaces saw significant wettability improvements with aggressive cleaning via HCl etching.

Key words: AM Copper, Solderability, SnPb, Pb-free, Additive Surfaces

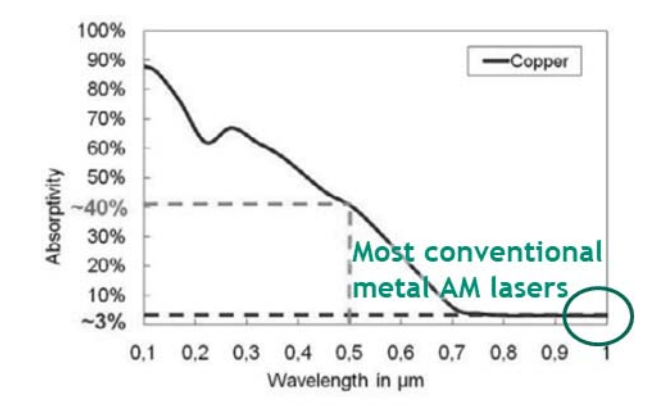
#### INTRODUCTION

# Additive Manufacturing with Copper

As with other materials, additive manufacturing (AM) of copper products increases design freedom. Complex, novel geometries involving nonlinear and/or tapered extensions (fins, blades), internal passages, and capillary wicking structures improves the capabilities to fabricate small, unique batches of components in thermal management, electrical, and jewelry applications [1-4]. Despite these design advancements supported by AM of copper, the AM process with copper has not seen the same technical progress as

other workhorse alloys such as aluminum, nickel, stainless steel, and titanium [5].

The lack of technical progress involving AM and copper is directly linked to copper's desired properties: thermal conduction and ductility [6-9]. Furthermore, copper has extremely low energy absorption (i.e., high reflectivity) at the conventional AM laser wavelengths ( $\approx$  1  $\mu$ m) (most metal additive processes use laser heat sources) accompanied by a step increase once melting occurs [10] as shown in Figure 1.



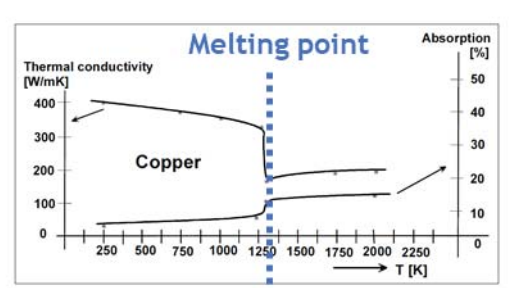


Figure 1: Absorptivity of copper at room temperature as a function of wavelength (left) and absorptivity and thermal conductivity as functions of temperature for copper at 1064 nm (right). [10, 11]

The low initial absorption and stepwise increase upon melting is problematic for 3 reasons: 1) reflected laser radiation can be dangerous to operators and damaging to the AM equipment itself; 2) the high thermal conductivity of copper makes the little radiation that is absorbed very inefficient at localized heating; and 3) the 10% absorption increase upon melting supports a very unstable melt pool that is difficult to maintain. In addition to the energy absorption challenges, the high ductility of copper means that the residual stresses between laser passes can cause significant distortion.

For these reasons, AM involving copper has evolved much more slowly than AM processes involving other metals. However, recent advancements involving copper alloying, laser wavelength variations, and processing have pushed the field into a regime where it is inevitable that laser AM production involving copper part fabrication will become a reality. Referring back to Figure 1, it is clear that shorter green ( $\approx 0.5 \mu m$ ) and blue ( $\approx 0.4 \mu m$ ) laser wavelengths have increased absorptivity by copper. Alloying copper with Ni, Si, Cr, and Zr has also proven effective at increasing the alloy absorption and conduction properties to provide a more stable melt pool. Of course, alloying comes at a cost, as it limits the final application of a given part. Alloyed copper no longer provides the thermal, electrical, and mechanical properties that generally warrants its use. Implementing pulse processing into existing and lower wavelength systems has also proven to minimize the heat conduction away from the melt pool [8]. Laser-based additive processes involving copper are limited in industry, but other printing methods involving sintering inks and paste layers are more established [8] [12].

These printing processes require liquid binders for applying the inks or pastes initially, and a final sintering step for fusing the copper powders while "burning off" the binder components, effectively leaving a pure copper coating behind. These methods are generally intended for 2-dimensional layer builds; however, 3-dimensional builds are possible. Ink printing/sintering-type processes are well-suited for electronic applications where 2D copper conduction pathways can be printed on for non-traditional circuitry [13]. Complicated 3D geometries can be fabricated with a binder jetting AM process [3].

It is plausible that both laser-based and ink-based additive manufacturing will become key processes to meet copper printing needs. Whether for structural or electronic applications, soldering these "as-built" surfaces during subsequent manufacturing steps is likely. The purpose of this study is to evaluate the solderability of various additively fabricated copper surfaces as this additive technology is evolving.

# Solderability

Solderability refers to the capability of molten solder filler metal to wet and spread over the base material surface, where wetting is the formation of a metallurgical bond and spreading is the spontaneous coverage by the molten solder and reaction layer. Identifying solderability behavior helps predict the immediate success of a given solder system used (liquid solder, base material, reaction layer, and flux). There are 3 typical solderability conditions: 1) wetting; 2) non-wetting; and 3) de-wetting, shown in Figure 2. Since the intermetallic layer is crucial to forming a complete metallurgical bond, wetting is the desirable condition. No metallurgical bond is formed in the case of non-wetting, and the de-wetting case lacks a continuous bond.

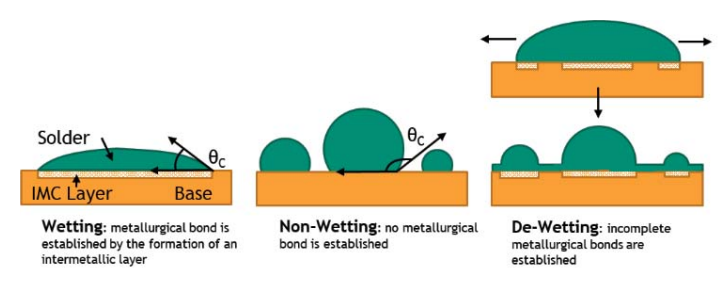


Figure 2: Schematic illustrating the three solderability conditions: wetting, non-wetting, and de-wetting.

Solderability also controls the final joint geometry, which can have long-term impacts on performance and reliability. Improper fillet size and significant void content will negatively impact performance and reliability of a given solder joint.

Solderability is often quantified by the contact angle ( $\theta$ C), calculated by Young's equation which relates the surface energies at the solid-flux, solid-liquid, and liquid flux ( $\gamma_{SI}$ ,  $\gamma_{SL}$ ,  $\gamma_{LI}$ , respectively). Contact angles for two solder-substrate orientations are shown in Figure 3. A wetting balance was used to calculate contact angles in this study.

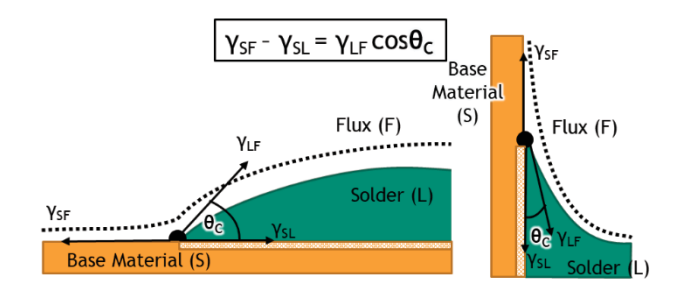


Figure 3: Schematic showing a molten solder drop in the sessile drop orientation (left) and molten solder in contact with a surface that is dipped into the solder (right).

It is conceivable that soldering additively manufactured surfaces, be it thin coatings or bulk components, will be required in an increasing number of products. It is therefore necessary to understand if and how different processing types impact solderability in order to provide input regarding process adjustments to improve solderability properties before these procedures become embedded in industrial processes. Both laser- and ink-based methods are of interest.

#### WETTING BALANCE TEST PROCEDURE

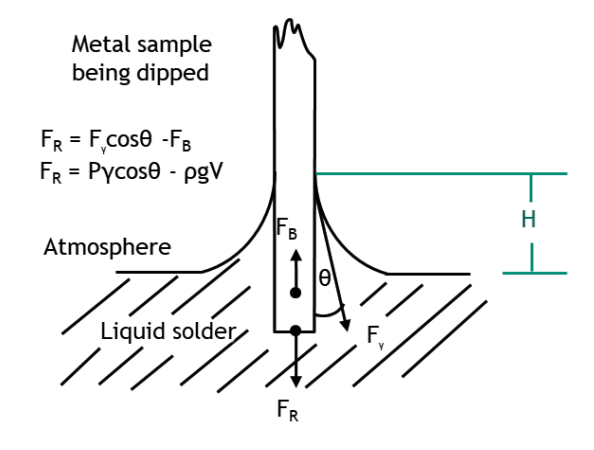
A wetting balance was used to compare the solderability of three types of AM Cu surfaces: 1) Thin AM coatings; 2) Laser processed surfaces; and 3) Bulk AM parts. For all surfaces, solderability was assessed for SnPb solder by measuring removal force and meniscus height for calculating contact angles and surface tension values. A limited solderability assessment was also performed regarding a Pb-free formulation, Sn-3.0Ag-0.5Cu (SAC305). AM surfaces were characterized before and after solder dipping via optical and electron imaging techniques.

Immediately prior to dipping, all coupons were ultrasonically rinsed in degreasing solvent trichloroethene (TCE) and subsequently in isopropanol (IPA) and air dried before applying a rosin mildly activating (RMA) flux. Coupons are typically etched in a 6M HCl solution to provide further oxide removal; however, AM coatings were not etched as the sample supply was low and etching degraded the coatings. All samples were therefore evaluated in the non-etched condition to remain consistent. The laser processed and bulk AM samples were also evaluated in the etched condition. Table 1 highlights this preparation step. Only the non-etched results are compared between all three sample types

Table 1: Samples contained within this study.

Sample Type	Etched	Not etched	
AM Coating		SnPb	
Laser Processed	SnPb	SnPb	
Bulk AM	SnPb, SAC305	SnPb, SAC305	

After cleaning, coupons were dipped 0.4 cm into the 245 °C (260 °C for Pb-free) molten solder at a rate of 5.0 mm/s, held for 10.0 s, and raised from the solder at a rate of 10.0 mm/s. Temperatures were chosen to mimic presently qualified processes and are relevant for typical electronic assembly reflow profiles in industry. Immediately after testing, coupons were cleaned using the same pre-dip cleaning procedure. A qualitative wetting curve and accompanying quantitative data are shown in Figure 4.



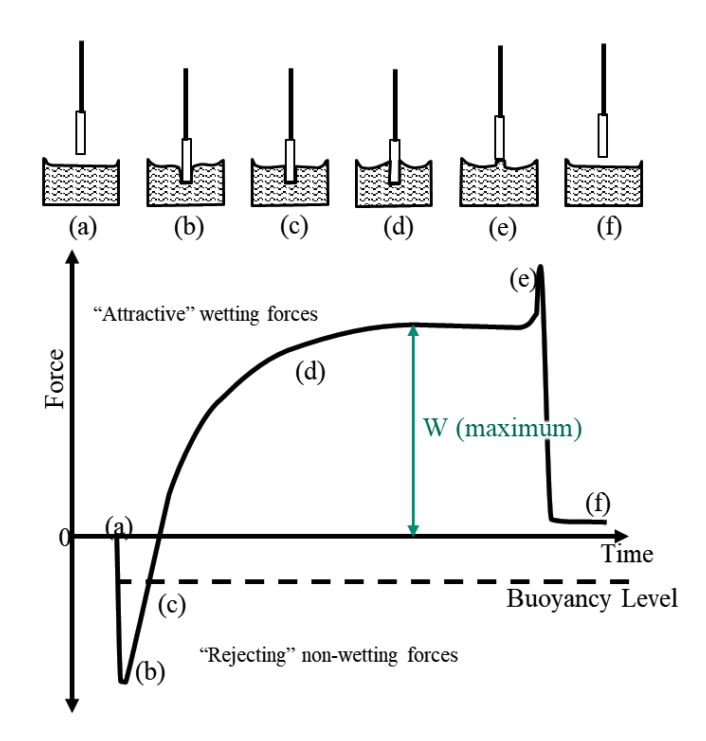


Figure 4: Schematic illustrating a solder dip (top) and the corresponding wetting curve (bottom), where  $\boldsymbol{F}_{_{R}}$  is the resolved downward force on the coupon,  $\boldsymbol{F}_{_{B}}$  is the buoyancy force,  $\boldsymbol{F}_{_{y}}$  is the meniscus force,  $\boldsymbol{P}$  is the cross-sectional perimeter of the coupon,  $\boldsymbol{\gamma}$  is the solder-flux interfacial energy,  $\boldsymbol{\rho}$  is density, g is gravitational force, and V is the volume of the immersed coupon.

## Metrics

Quantitative and qualitative evaluation accompanied each coupon dip. The wetting balance technique allows experimental measurement of the meniscus height and weight, from which other parameters such as contact angle, solder-flux interfacial tension, wetting rate, and wetting time can be measured/extracted. Meniscus heights were manually measured post-test while meniscus weight values were measured in-situ. In addition, a post-dip solder assessment provided qualitative interpretation for each dip.

# Qualitative Coupon Evaluation

Images of dipped coupons were compared to evaluate general wetting trends for each sample type and confirm that the wetting balance data is accurately portraying solderability performance. Etched and unetched conditions were compared for the traditional, laser-processed, and bulk AM surfaces.

#### Quantitative Metric Evaluation

Force vs. time curves were used to quantitatively evaluate the samples. Five samples were dipped, and the five curves for each condition were averaged and compared to evaluate obvious, qualitative differences.

#### Contact Angle

Contact angles are often used as a general measure of wettability because they reflect a resultant interaction between the three interfacial tensions (related through Young's equation) present during liquid wetting of a solid substrate, as shown in Figure 5. Contact angles were calculated using Equation 1. A complete derivation can be found by Mayhew and Monger [14, 15].

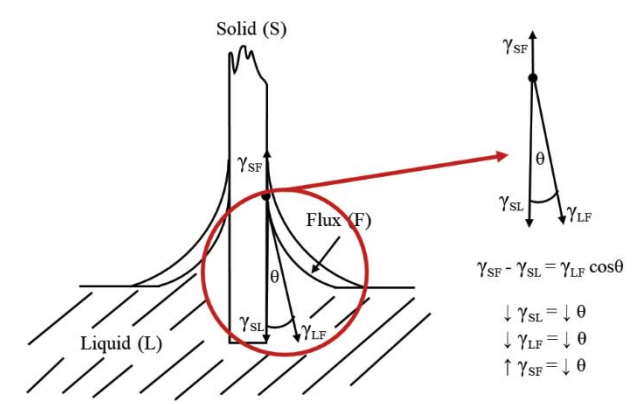


Figure 5: Interactions between solid-flux (SF), solid-liquid (SL), and liquid-flux (LF) interfacial tensions when a solid is coated with a flux and dipped into molten solder (left). The relationship between these interfacial tensions as defined by Young's equation is shown on the right.

$$\theta_{Ci} = sin^{-1} \left[ \frac{4W^2 - (\rho g P H^2)^2}{4W^2 + (\rho g P H^2)^2} \right]$$
 (1)

 $\theta_{C,i}$  Contact Angle (°)

W Meniscus Weight (dynes)

ρ Liquid solder density (g/cm<sup>3</sup>)

g Acceleration due to gravity (cm/s<sup>2</sup>)

P Cross-section perimeter (cm)

H Meniscus height (cm)

Lower contact angles are associated with better wetting performance and are minimized when the solid-liquid and liquidflux energies are minimized as the solid-flux energy is maximized. Conceptually, this makes sense because if the solid-flux interfacial energy is the highest of the three, it is also the "least preferred" or least stable. Systems tend to "move" toward the lowest and most stable energy configuration possible. In this case, the "system" refers to the solid coupon, the flux on the coupon surface, and the molten solder. If the solid-flux interfacial energy is lower than the other two, there will be no driving force for the liquid solder to wet the solid substrate because the interfacial energy would not decrease upon doing so; therefore, fluxes must exhibit lower interfacial energies with liquid solder than the solid substrate to promote wetting. Lower solid-liquid and liquid-flux interfacial energies create a scenario in which liquid solder travels between the flux and the solid, thereby replacing the higher energy solid-flux interface with the lower energy, more preferred solid-liquid interface. Table 2 shows the generally accepted wetting trends associated with contact angles [16].

Table 2: Wetting behavior categories associated with contact angle ranges.

Contact Angle (°)	Wetting Behavior		
0-10	Perfect		
10-20	Excellent		
20-30	Very Good		
30-40	Good		
40-55	Adequate		
55-70	Poor to Fair		
70-90	Very Poor		
90	No Wetting		

Note that it is possible for Equation 1 to return negative contact angle values when the meniscus height absolute value, |H|, is sufficiently large. The expression below identifies the conditions required to calculate a negative contact angle where  $\varrho$  is about 7-10 g/cm³ (for a range of solder compositions), g is  $980 \text{cm/s}^2$ , and P ranges from 3-5 cm (depending on sample geometry).

$$0 < W < \frac{H^2 \rho g P}{2} \tag{2}$$

In the context of this study, when W is both greater than zero and less than 110H-143H a negative contact angle can be calculated. If H becomes sufficiently large, these conditions are more likely to be met. A large, positive H value indicates excellent wetting, while a large negative H value indicates no wetting, as shown in Figure 6.

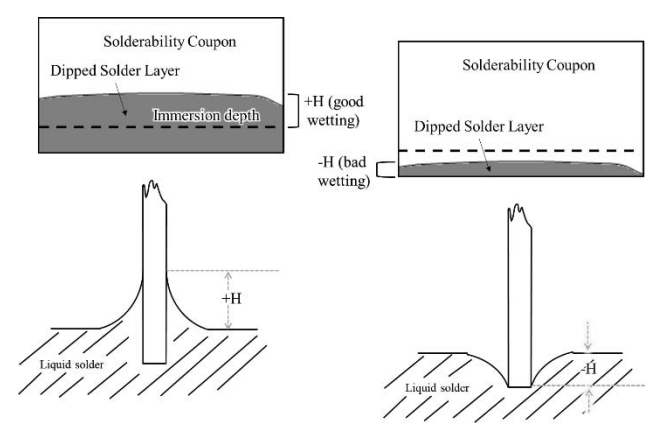


Figure 6: Schematic illustrating a positive (left) vs. negative (right) meniscus height.

Negative contact angles can therefore represent both extremely good and extremely bad wetting scenarios without distinction. To eliminate confusion, when negative H values were measured, they were recorded as 0. By default, a contact angle of 90° is returned, which signifies poor wetting. Any negative contact angles reported in this study therefore indicate excellent wetting.

Another testing condition can occur if different coupon sides wet differently. If meniscus height values vary significantly between the left and right sides, non-symmetrical forces from asymmetrical menisci could cause a net sample tilt as illustrated in Figure 7. A significant tilt would cause a discrepancy between the actual contact angles and those calculated with Equation 1.

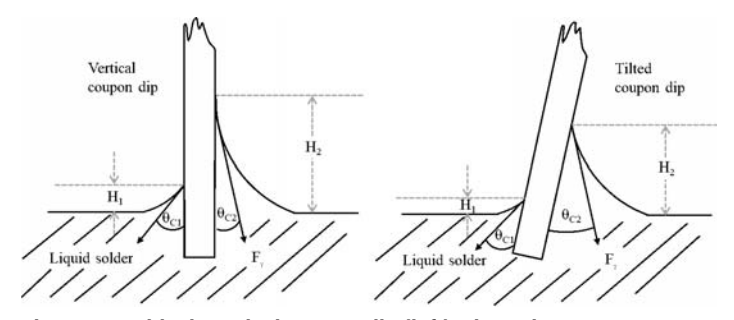


Figure 7: An ideal, vertical coupon dip (left) where the correct contact angles can be calculated, and a tilted coupon dip (right) where the calculated contact angles would not represent the actual contact angles.

Vianco [14] took asymmetric sample tilting into account to verify the integrity of the wettability data. Though wetting variations between the 2 sides were recorded, the differences were not great enough to significantly impact the data; that is, the possible error due to asymmetric wetting was not larger than the experimental error associated with the testing apparatus [14]. Due to the similarities between Vianco's previous study and the current study, and the fact each side is the same material and fabricated with the same process, the same assumption is made for this study.

# Solder-Flux (Liquid-Flux) Interfacial Tension

While contact angle values reflect the interaction between the three interfacial energies (Surface-Flux, Surface-Liquid, Liquid-Flux) as described by Young's equation, it is also useful to assess each individual interfacial energy. Based on the empirical measurements meniscus weight (W) and meniscus height (H), only the solder-flux interfacial energy can be calculated via Equation 2. This mathematical relationship is derived elsewhere [14, 15].

$$\gamma_{LF} = \frac{\rho g}{4} \left[ \frac{4W^2}{(\rho g P H)^2} \right] + H^2 \tag{3}$$

γ<sub>LF</sub> Liquid-flux surface tension (dynes/cm)

W Meniscus Weight (dynes)

ρ Solder density (g/cm³)

g Acceleration due to gravity (cm/s2)

P Cross-section perimeter (cm)

H Meniscus height (cm)

As meniscus weight and/or meniscus height decrease, the interfacial energy increases and solderability decreases. Since flux and solder composition remained constant in this study, the solder-flux interfacial tensions should be similar. Differences could occur, though, depending on dissolution of the substrate into the liquid, thereby changing the solder composition. Note that as meniscus height values approach 0, the interfacial energies approach 0 (i.e. infinitely poor wetting). For the samples where negative H values were input as 0 to avoid a negative contact angle, the resulting interfacial energies are infinitely high.

# **AM SURFACES**

# AM Copper Coatings

Four additive copper coatings were evaluated. Each coating was applied to 25.4 x 25.4 x 0.51 mm oxygen free high conductivity (OFHC) coupons manufactured by Intrinsiq<sup>TM</sup> (since merged with Novacentrix®). All formulations are proprietary.

1. CP-007 Conductive copper paste: General-purpose high-performance screen print.

The paste was applied to one side of the copper coupon (Top or "T-side") and sintered at 230 °C. The same procedure was then performed on the opposite side (Bottom or "B-side").

2. CP-008 Conductive copper paste: High copper, low temperature screen print.

The procedure used for CP-007 was repeated for this paste.

3. IMC-4118 Copper conductive laser sinter paste.

The paste was screen printed using a Dek printer and individually dried in a box oven for each coupon side. Laser sintering normally follows; however, in this case laser sintering was unsuccessful due to the significant heat absorption by the copper coupon under the paste. Each side was instead cured at 400 °C in an inert atmosphere containing formic acid as a reducing agent.

4. IMC-2501 Copper ink. Fabrication and application details are proprietary.

Figure 8 shows images of the four layer types, as-coated.

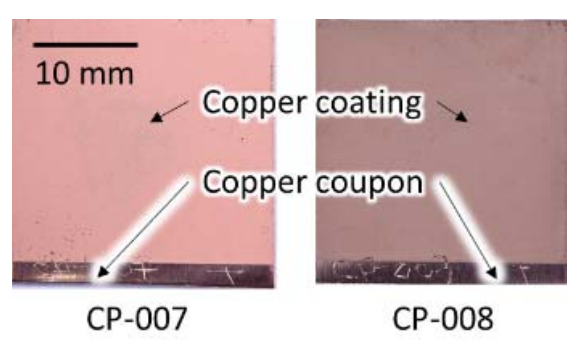


Figure 8: As-coated images of the 4 different copper layers on a copper coupon.

From this macroscopic scale, both sides of a given coupon appear nearly identical. With the naked eye, all coatings appear similar except the IMC-2501 coating. Uneven coloration and cracking in the layer are shown in Figure 9.

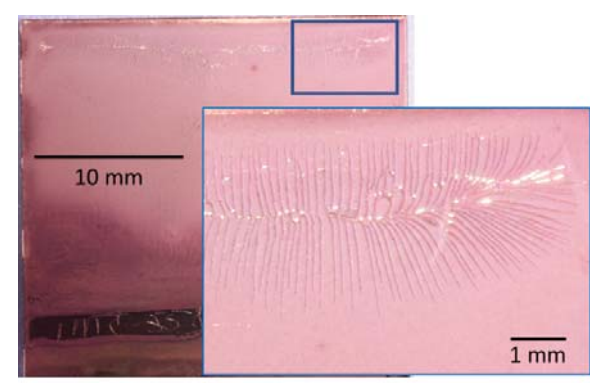


Figure 9: Image highlighting a region on the IMC-2501 coating surface where a "featherlike" coating defect is visible.

Representative SEM images of the four coating surfaces are shown in Figure 10.

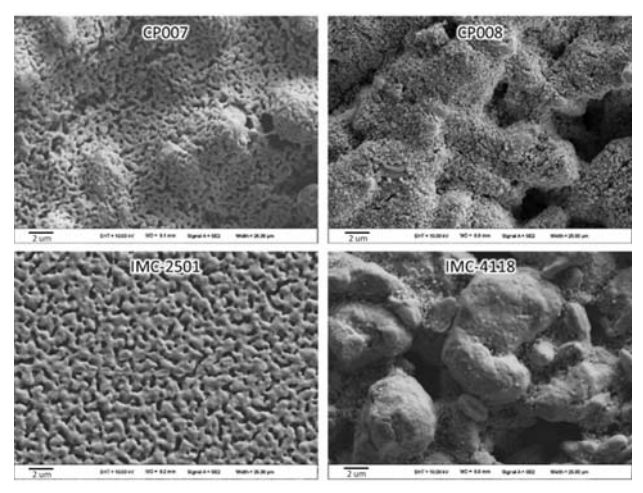


Figure 10: SEM images depicting the surface morphologies of the four different coatings.

The CP007 and CP008 surfaces are comparable. IMC-4118 appears relatively coarse and exhibits large uncoalesced particles. The IMC-2501 coating shows a fine coalesced network. Cross-sections through the coatings also reveal differences between the layers. SEM images show the coupon cross-sections in Figure 11.

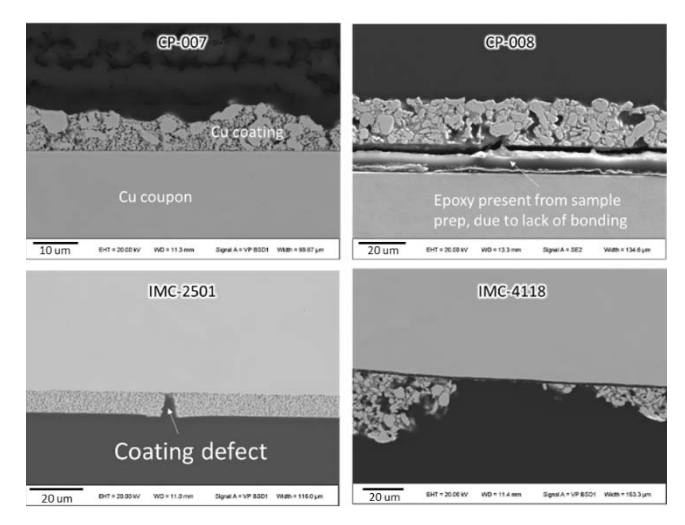


Figure 11: SEM backscatter images of the cross-sections. Note the different scales.

The lack of bonding revealed in the CP-008 surface rendered it unfit for the solder dipping wetting balance test, as the surface disintegrated during the cleaning process. As such, all results reflect only the CP-007, IMC-2501, and IMC-4118 coatings.

## Laser Processed Copper Surfaces

Laser processed coupons were fabricated by subjecting the top and bottom surfaces of a typical Cu sheet coupon (25.4 x 25.4 x 0.51 mm) to laser remelting. The purpose of this laser processing was to generate a microstructure and surface finish representative of other laser AM processes by exposing the surface to representative, rapid melting and cooling rates. An IR (1.064  $\mu$ m) fiber laser with galvanometric laser scanning in conduction mode generated a shallow melt pool on the surface, that did not penetrate through the coupon. Laser processing occurred under the application of argon (Ar) gas. Horizontal passes were made at the end of the coupon to be dipped in solder, and the laser rastered through both a linear pattern and a circular pattern to produce two unique samples. The schematic in Figure 12 illustrates the fabrication of the laser processed samples, Figure 13 highlights the processed surfaces, and Figure 14 shows an optical image of a cross-section.

16

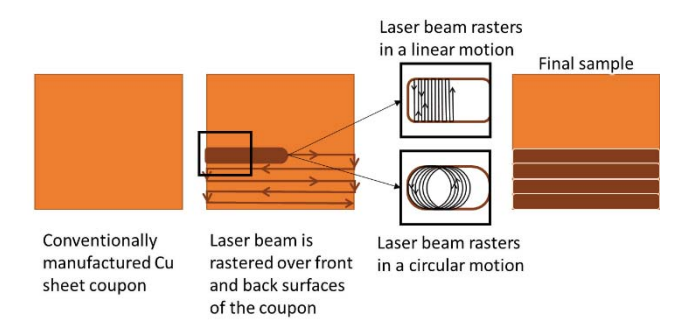


Figure 12: Schematic of the laser processing technique.

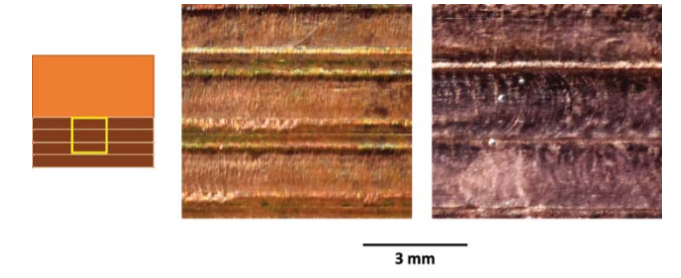


Figure 13: Optical images of the processed surfaces for the linear (middle) and circular (right) scans.

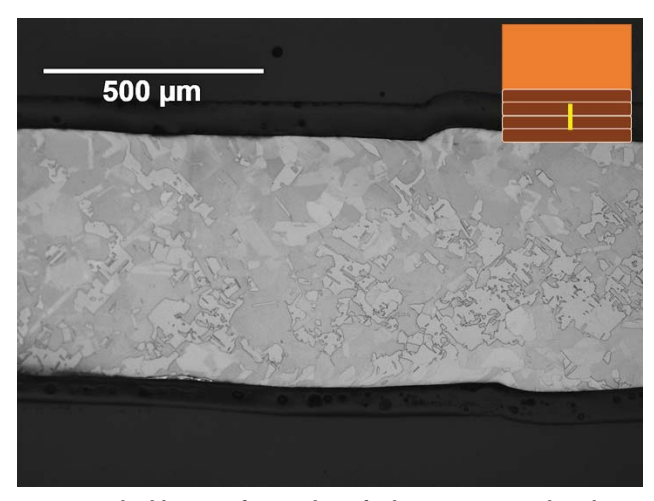


Figure 14: Optical image of a section of a laser-processed region, cross-section location shown on the inset schematic.

# **Bulk Additively Manufactured Copper Coupons**

Bulk AM coupons were produced by a laser-based powder-bed process. To simulate as-built AM surfaces, pure Cu solderability coupons (25 x 15 x 0.5 mm) were fabricated and provided by TRUMPF Inc<sup>TM</sup> with a TruPrint 1000<sup>TM</sup> green wavelength laser additive manufacturing machine. Figure 15 illustrates an as-received sample. Note that burs and sharp edges were filed to reduce their impact on solder wetting as would be done with traditional Cu coupons.



Figure 15: Coupons were built as thin walls in the direction of the blue arrow.

The main interest in this study is in the as-built surface condition. Complicated parts involving internal cavities, lattices, or printed conduction surfaces whose cleaning may be limited by the circuitry materials would have to be soldered in the as-built, or as-printed, condition.

Scanning electron microscopy (SEM) was used to characterize the AM surface as well as sample cross-sections as shown in Figure 16 and Figure 17, respectively.

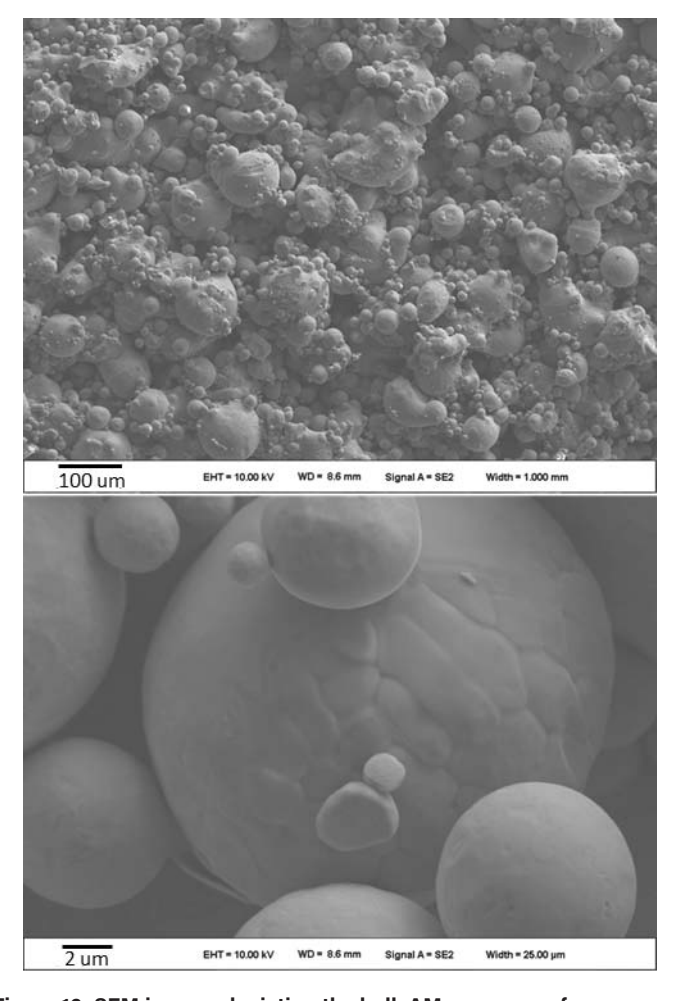


Figure 16: SEM images depicting the bulk AM coupon surface.

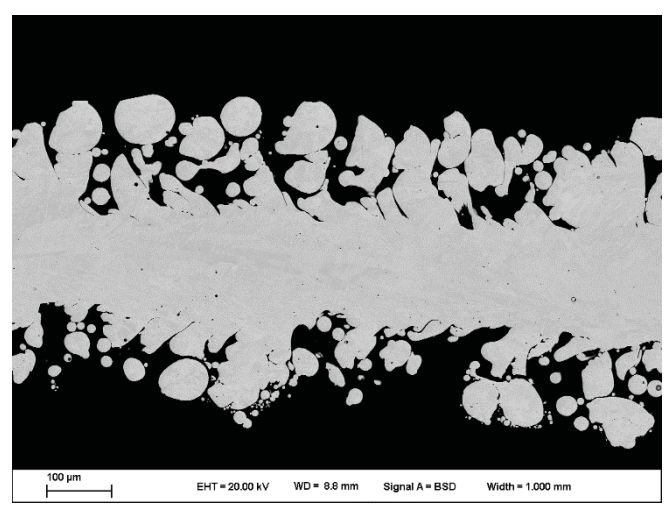


Figure 17: SEM image of a longitudinal cross-section taken through the bulk AM coupon.

The typical as-built AM surface morphology may be a factor that influences solder wetting. Other factors may include the impact of the fast cooling rate on surface energy and porosity.

The cross-section reveals that the coupon exhibits a dual microstructure in the through-thickness direction.

Figure 18 highlights the grain structure in both longitudinal and transverse cross-sections with electron backscatter diffraction (EBSD) maps.

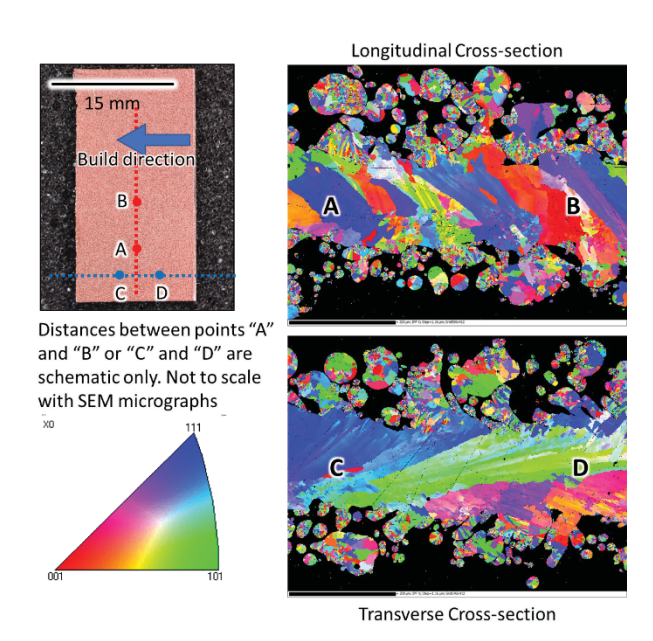


Figure 18: EBSD maps along longitudinal (top) and transverse (bottom) sections of a bulk AM coupon.

#### **WETTABILITY RESULTS**

#### **Qualitative Coupon Evaluation**

Representative images of unetched and etched samples after dipping in SnPb solder are shown in Figure 19 and Figure 20, respectively.

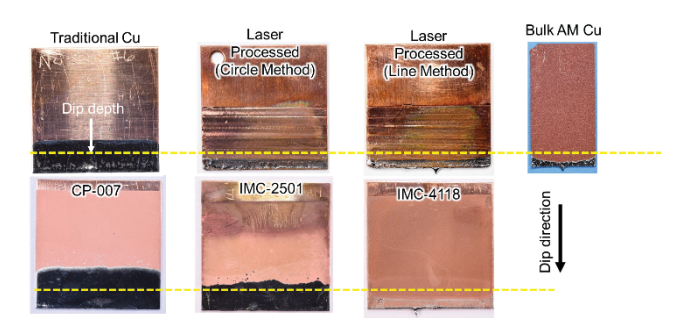


Figure 19: Representative images depicting unetched samples postdip, with SnPb solder. The yellow dotted line indicates the dip depth.

Only the traditional Cu, CP-007, and IMC-2501 exhibit a positive meniscus height, (i.e. wetting beyond the dip depth) without etching.

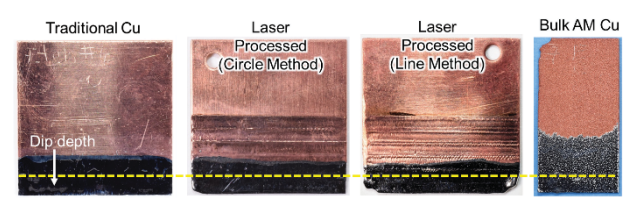


Figure 20: Representative images depicting *etched* samples post-dip, with Sn-Pb solder. The yellow dotted line indicates the dip depth.

All 4 samples exhibit a positive meniscus height. The spreading improves on all samples with the Bulk AM sample showing the most significant improvement compared to the unetched condition.

#### **Quantitative Metric Evaluation**

Average wetting curves corresponding to each sample type are shown in Figure 21. Calculated contact angles, interfacial energies, and wetting rates are shown in Table 3. From this chart, good wetting is exemplified by low contact angles, low L-F energies, and high wetting rates. Conversely, poor wetting is exemplified by high contact angles, high L-F energies, and low wetting rates. The rows highlighted in red indicate instances where the meniscus height, H, was sufficiently low to assume a contact angle of 90°, which drives the surface tension,  $\gamma_{\rm LP}$ , to mathematically approach infinity (see Equation 1).

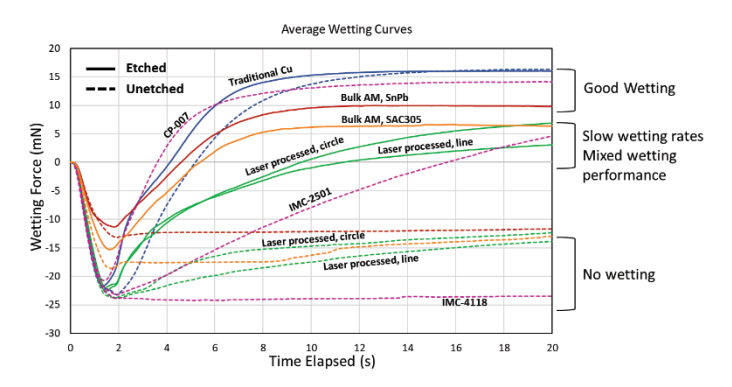


Figure 21: Average wetting curves for the traditional Cu sheet (blue), laser processed (green), AM coatings (pink), and bulk AM samples (red and orange). Solid lines indicate etching prior to dipping; dashed lines indicate no etching prior to dipping.

Table 3: Contact angles, liquid-flux interfacial energies, and wetting rates for each sample type. Error of one standard deviation is provided.

Sample		Contact Angle	Surface Energy	Wetting Rate	
Туре	Solder	Etch?	(degrees)	L-F (dynes/cm)	(mN/sec)
Traditional (Wrought) Cu	SnPb	Υ	19.6 ± 3.5	421.9 ± 13.8	13.3 ± 1.0
		N	13.9 ± 6.4	411.8 ± 15.9	$7.6 \pm 0.4$
Bulk AM	SnPb	Υ	-47.5 ± 3.2	673.9 ± 43.4	4.4 ± 0.2
		N	90	Infinite	$\textbf{0.7} \pm \textbf{0.1}$
Bulk AM	SAC305	Υ	61.1 ± 5.0	678.2 ± 57.0	4.3 ± 0.4
		N	90	Infinite	$\textbf{2.8} \pm \textbf{0.8}$
Laser (Line)	SnPb	Υ	70.9 ± 18.3	849.9 ± 264.3	6.1 ± 2.9
		N	84.1 ± 5.9	10290.0 ± 504.2	$1.0 \pm 6.1$
Laser (Circle)	SnPb	Υ	56.1 ± 33.7	19374.0 ± 19028.0	6.9 ± 4.9
		N	79.9 ± 11.4	2025.8 ± 1934.1	2.0± 0.7
CP-007 Screen	SnPb	N	-4.1 ± 28.0	423.7 ± 35.4	10.4 ± 2.1
CP-008 Screen	SnPb	N	Complete Coating Delamination - No Test		
IMC-2501 Vapor	SnPb	N	30.7 ± 20.6	257.9 ± 109.1	$1.9 \pm 0.4$
IMC-4118 Screen	SnPb	N	90	Infinite	0.3 ± 0.4

Figure 22, Figure 23, and Figure 24 graphically show the data from Table 3.

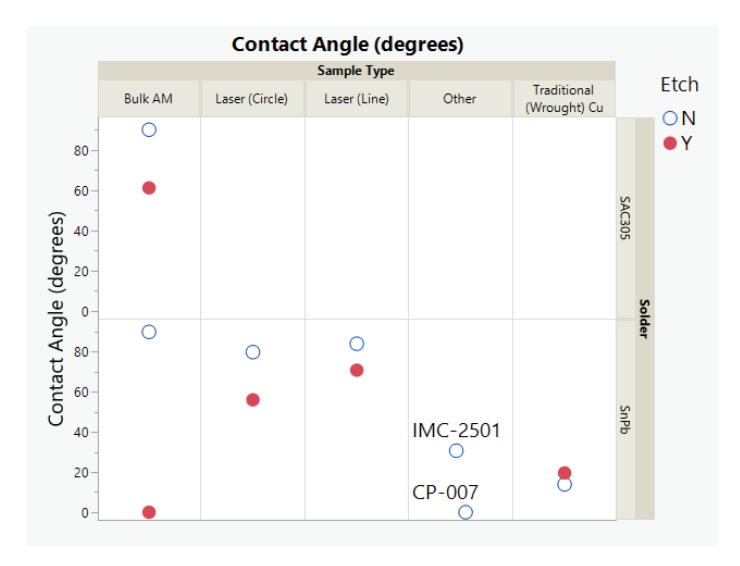


Figure 22: Contact angles for the sample types tested.

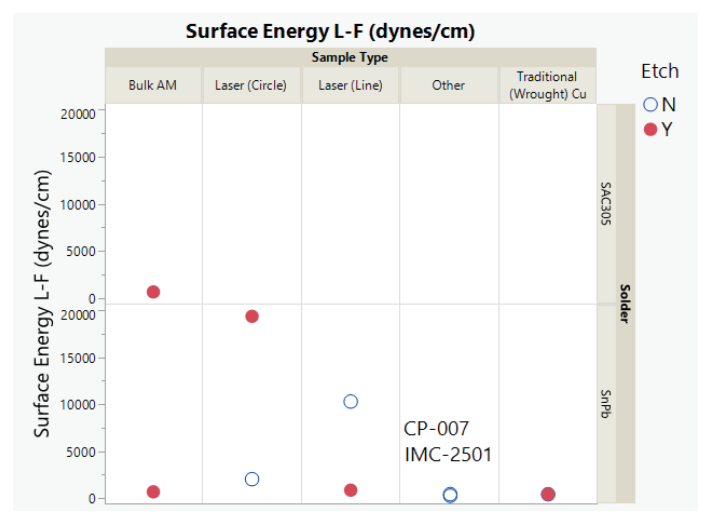


Figure 23: Surface energy values for the sample types tested.

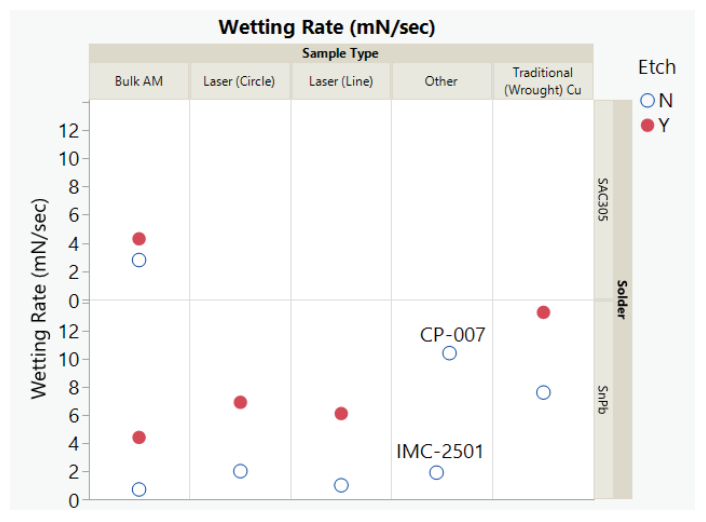


Figure 24: Wetting rate values for the sample types tested.

# Effect of Surface Type

Traditional Cu samples behaved as expected, exhibiting excellent wetting.

Performance varied for each printed Cu coating type. CP-007 exhibited a negative contact angle (very positive meniscus measurement), an L-F surface energy comparable to the traditional Cu surface, and a wetting rate comparable to the traditional Cu surface. IMC-2501 produced good contact angles, lower L-F energies than traditional Cu, but slow wetting rates. IMC-4118 was the worst performer for all 7 surface conditions, exhibiting no wetting or spreading.

The laser processed samples exhibited adequate wetting at best. Contact angles and surface energies were generally high. Significant differences between the circular and linear motions were not apparent.

The bulk AM samples supported both excellent and terrible wetting. Wetting rates were relatively low. The surface energies for the samples that wet were still above those of traditional Cu.

# Effect of Etching

Etching produced better wetting for all the samples exposed to the step (Cu coatings were not studied in the etched condition). Etching had the smallest effect on the traditional Cu samples, both conditions producing similar contact angles and surface energies; however, the wetting rate nearly doubled. Both the laser-processed and bulk AM samples exhibited effectively no wetting or spreading in the unetched condition. Contact angles and surface energies improved slightly upon etching for laser-processed samples, but both values improved drastically for the bulk AM samples. Etching did produce moderate wetting rates for the laser processed samples, relative to the unetched sample set. Authors hypothesize that residual weld soot that often remains after laser processing (due to plasma plume interacting with and vaporizing base material) is likely more effectively removed with the etch, compared to the standard cleaning procedure.

# Effect of Solder Composition

SAC305 was only evaluated for the bulk AM samples. Surface energies and wetting rates were similar between SnPb and SAC305 compositions, but the contact angle is much lower for SnPb. The negative contact angle for SnPb indicates a very high meniscus height, H, measurement. The contact angle for SAC305 indicates fair wetting. For both solder compositions, the wetting rates are slower than those measured on traditional Cu, and the surface tension values are higher. Composition often has an intrinsic role in wetting behavior, but solder pot temperature may need to be assessed, as temperature optimization was not investigated, here. Practically, higher reflows than 260°C often cannot be supported in electronic assembly and production lines.

#### **CHARACTERIZATION**

SEM images of the coupons post-solder dipping are shown in Figure 25, Figure 26, and Figure 27. A macroscopic comparison between SnPb and the Pb-free composition, SAC-305, is shown in Figure 28.

# **Bulk AM** Cu

Signal A = BSD

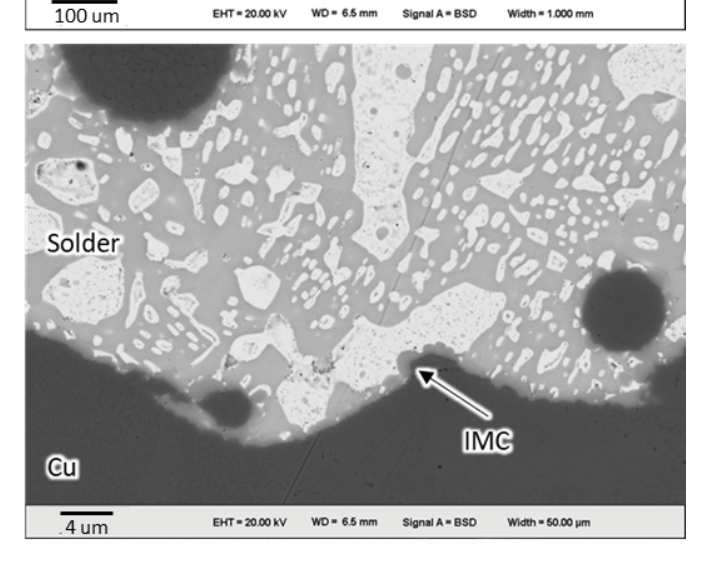
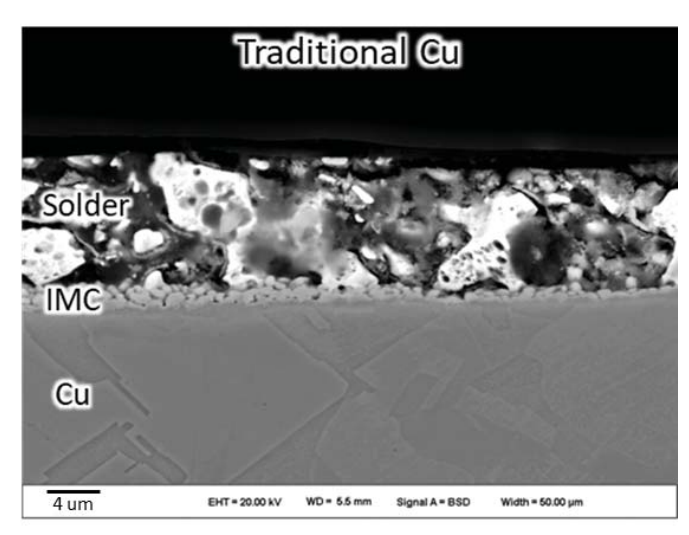


Figure 25: Low and high SEM magnifications of a bulk AM Cu coupon (etched) dipped in Sn-Pb solder, top and bottom, respectively.

Solder wets throughout the majority of the AM coupon's intricate surface. A majority of the sub-surface cavities and tortuous, circuitous pathways support solder wetting. Scalloped intermetallic formation along the copper-solder interface is confirmed, indicating a wetting reaction.



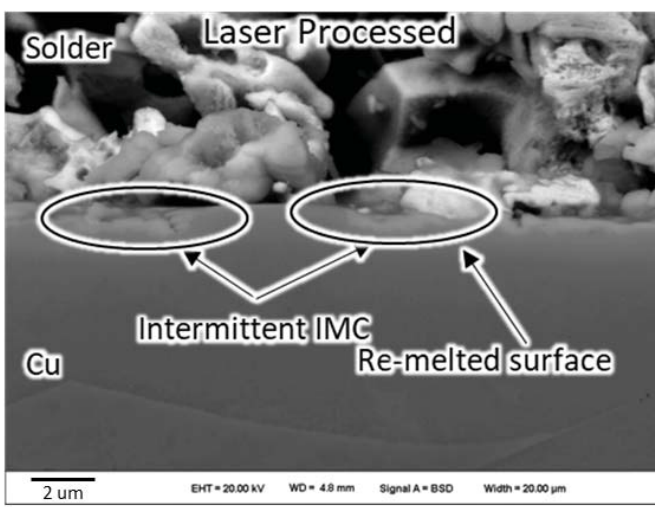
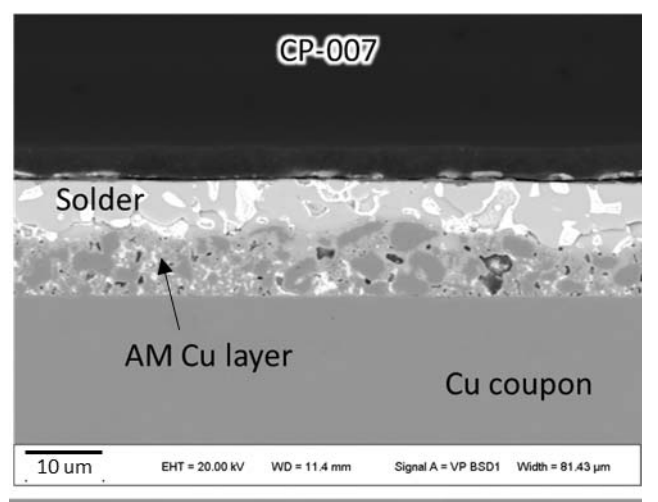
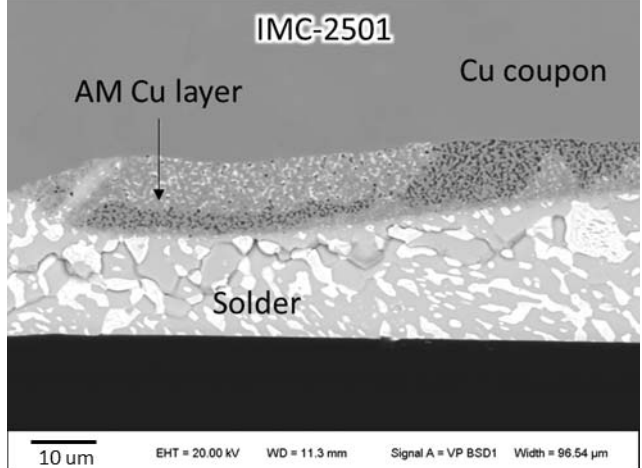


Figure 26: SEM images depicting the solder-copper interfaces for a traditional Cu coupon (top) and a laser processed coupon (bottom). Both cross-sections were etched, which destroyed the integrity of the SnPb matrix, but more clearly shows the base Cu structure and the IMC.

The interfacial structure of the traditional coupon is typical for a Sn-Pb solder on Cu where a continuous intermetallic is observed. A continuous intermetallic is not observed in the laser processed sample.





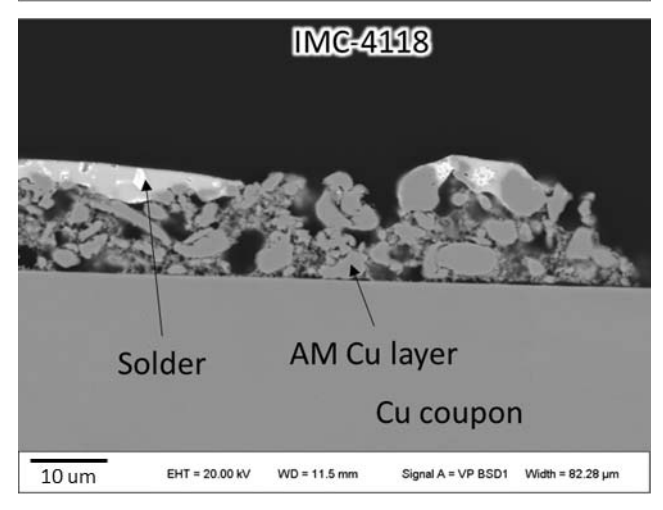


Figure 27: SEM images, post-dipping (SnPb), showing the solder interaction with each coating.

Surface solder wetting and nearly complete penetration within the Cu coating is observed in CP-007. A high fraction of intermetallic compound is expected. Surface solder wetting and inconsistent solder penetration into the Cu coating is observed for IMC-2501.

Limited surface wetting and no penetration into the coating is observed for IMC 4118.

When considering SnPb vs. Pb-free, the Pb-free solder does wet and spread, but appears to accumulate soon after wetting where the Sn-Pb solder continues spreading up along and through the bulk AM surface as shown in Figure 28.

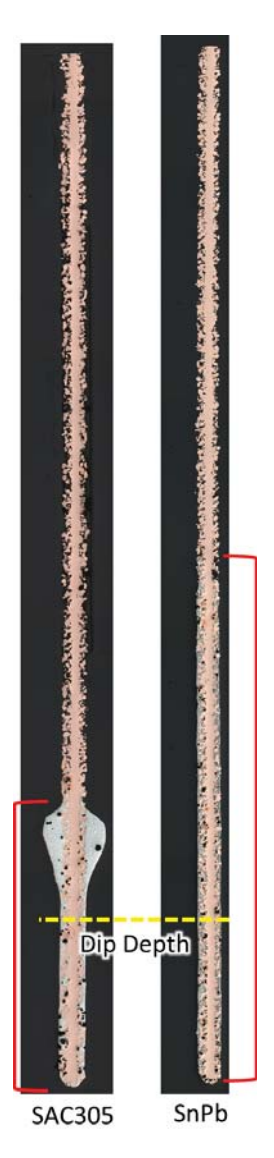


Figure 28: Optical images of bulk AM cross-sections after dipping for Sn-Pb (right) and Pb-free (left). Red brackets indicate the total travel of solder up the coupon.

#### **DISCUSSION**

Even though all examined surfaces are meant to represent pure copper, the wetting behavior is very different, ranging the full gamut from no wetting to exceptional wetting. Surface morphology, geometric considerations, contamination, and other fabrication processing parameters may play important roles in an end product's surface solderability.

# Effect of Sample Type

Traditionally manufactured Cu sheet remains a top performer.

At least one of the Cu-printed coatings is also a top performer; however, the variability in wetting and spreading among these Cu coatings suggests a strong correlation between processing and solderability. Contamination from each coating process could limit solderability. Residual components from binder materials in a printed paste may play a role as well. Since the processing for these 3 coatings is largely proprietary, identifying the key process parameters, associated mechanisms for promoting vs. inhibiting wetting and spreading, and high-level correlations is difficult.

Similar to the printed Cu coatings, the fair-to-poor solderability of the laser-processed surfaces suggests a correlation between processing and wetting behavior. The Cu substrate that underwent laser processing was from the same lot of traditional Cu used in the study; exposure of the coupon to the laser likely altered the equilibrium state between substrate, solder, and flux surface energies. Small composition changes might be occurring if the melt pool is exposed to potential contamination.

The bulk AM samples that wet well exhibited solder penetration through the porous structure as the solder climbed the coupon. The surface area that reacted with the solder was likely much greater than the surface area that reacted for the smooth, flat, traditional Cu coupon. This increased fraction of reaction layer could have several performance implications: 1) the likelihood of low-load interfacial failure may be reduced since the solder-Cu interface is more intricate compared to a straight line; 2) electrical performance may be impacted if conductivity changes due to an increased fraction of interfaces; 3) the volume fraction of intermetallic compound likely increases, potentially increasing the number of brittle stress concentration locations; and 4) the weight of the solder joint will likely increase as the solder fills porous cavities. Evaluating bulk AM joint performance against traditional joint performance in terms of mechanical integrity over time would be a useful complement to this current study.

For the quantitative data, it is important to consider how the evaluation is impacted by the surface morphology of AM surfaces. For calculations of contact angle and interfacial tension, the measured solder weight and meniscus height values are used. Normally, the weight of the solder is attributed to the solder within the volume of the meniscus; however, with an intricate morphology like the bulk AM coupons, a significant portion of the solder volume may be attributed to the solder that penetrates into the cavities AND the solder that makes up the meniscus shape. So, the weight-to-meniscus height values for AM surfaces might be much greater than for traditional smooth surfaces.

Understanding the solderability of a given coating is key before designing that coating into an electronic assembly.

# Effect of Etching

Etching the copper samples improved wetting and spreading of all samples which were etched. Etching increased the wetting rate (kinetics) for traditional Cu samples but did not significantly affect the contact angle (thermodynamics), suggesting that the flux action

is sufficient (but slower) at removing surface contamination/oxides.

The fact that the laser processed surfaces only marginally improved upon etching suggests that contamination may have been introduced to the melt pool and solidified into the surface, even under Ar atmosphere; etching and cleaning would not remove any contamination or oxides which solidified into the melt pool.

The fact that the bulk AM samples exhibited the most drastic change from non-wetting to sometimes extreme wetting speaks to the difficulty for effective flux cleaning of the porous surface structure. Soldering as-fabricated AM surfaces may warrant aggressive surface preparation. In applications where aggressive cleaning may damage other parts, implementing AM solder joints may prove difficult. Etching with HCl is aggressive and not a traditional cleaning step on an electronics assembly line, for example.

# Effect of Solder Composition

SnPb solder performed better than SAC305 on bulk AM surfaces, suggesting a greater sensitivity of the Pb-free formulation to surface morphology and cleanliness condition.

The accumulation of SAC305 compared to the even penetration and rise of the SnPb solder for the bulk AM samples is interesting and may require further study. While the SAC305 was heated to 260 °C relative to the SnPb at 245 °C, it is conceivable that differences in the thermal gradient may have impacted wetting for each.

#### **CONCLUSION**

Solderability was evaluated over a range of AM-like surfaces for 63Sn-37Pb solder. A limited evaluation for Pb-free SAC305 was performed for the bulk AM samples. The main conclusions are listed below:

- 1. Surface type played a role in the solderability. Traditional Cu coupons provided the control data and were a top performer. One coating (CP-007) rivaled traditional Cu for solderability performance, and bulk AM samples ranged between excellent wetting and terrible wetting. Laser processed surfaces did not wet well.
- 2. Etching significantly impacted solderability performance for bulk AM samples, marginally impacted solderability for laser processed samples, and minimally impacted solderability for traditional coupons.
- 3. Solder composition affected solderability. For aggressively cleaned and etched samples, solderability of bulk AM samples was excellent with SnPb and marginal with Pb-free.
- 4. At a high level, additive surfaces, even when intended to be pure Cu, do not necessarily support solder wetting like a traditionally manufactured Cu surface. Additional work should focus on the specific mechanisms that inhibit or promote solderability in relation to AM processing.

#### **ACKNOWLEDGEMENTS**

Authors would like to acknowledge TRUMPF  $^{\! {\rm TM}}$  for providing the bulk AM samples.

#### **REFERENCES**

- 1. Frigola, P., Fabricating Copper Components with Electron Beam Melting. 2014.
- 2. ILT, F.I.f.L.T., Additive Manufacturing of Copper Components with Selective Laser Melting. 2011, Fraunhofer Institute for Laser Technology ILT.
- 3. Gradl, P.R., et al. "Progress in Additively Manufactured Copper-Alloy GRCop-84, GRCop-42, and Bimetallic Combustion Chambers for Liquid Rocket Engines." 70th International Astronautical Congress (IAC), Washington, DC. 2019; Available from: www.nasa.gov.
- 4. C. Kaestle, e.a. Evaluation of Influencing Factors on the Heavy Wire Bondability of Plasma Printed Copper Structures. in 17th Electronics Packaging Technology Conference. 2015.
- 5. Murr, L.E., A Metallographic Review of 3D Printing/Additive Manufacturing of Metal and Alloy Products and Components. Metallography, Microstructure, and Analysis, 2018. 7: p. 103-132.
- 6. Lee, M., N. Reinermann, and M. Grupp. Welding of Copper with brilliant fiber laser sources. in 9th International Conference on Photonic Technologies LANE. 2016.
- 7. Keller, C., Processing of Highly Reflective Materials. Laser Technik Journal, 2017: p. 30-33.
- 8. Kaden, L., et al. Additive Manufacturing of pure copper using ultrashort laser pulses. in SPIE LASE 2019. San Francisco.
- 9. Engler, S., R. Ramsayer, and R. Poprawe, Process Studies on Laser Welding of Copper with Brilliant Green and Infrared Lasers. Physics Prodedia, 2011. 12: p. 339-346.
- 10. Blom, A., et al. Process spread reduction of laser microspot welding of thin copper parts using real-time control. in High Power Lasers and Applications. 2003. San Jose, CA.
- 11. Hess, A., et al., Continuous Wave Laser Welding of Copper with Combined Beams at Wavelengths. Physics Procedia 2011. 12: p. 88-94.
- 12. Tran, T., A Review: Additive Manufacturing for Active Electronic Components. Virtual and Physical Prototyping, 2016.
- 13. Espalin, D., et al., 3D Printing multifunctionality: structures with electronics. Int J Adv Manuf Technol, 2014. 72: p. 963-978.
- 14. Vianco, P.T., F.M. Hosking, and J.A. Rejent, Wettability of Metallic Glass Alloys by Two Tin-Based Solders. Welding Journal, 1994.
  - 15. Mayhew, A. and K. Monger. in NEPCON. 1972.
- 16. Mayhew, A.J. and G.R. Wicks. Solderability and Contact Angle. in Proceeding International Nepcon III. 1971.

#### **BIOGRAPHIES**

Rebecca Wheeling is currently Principal Weld Engineer/ Metallurgist in the Joining Development sector of Medtronic Inc. She previously worked as a Senior Member of the Technical Staff at Sandia as part of the Metallurgy and Materials Joining group. She has a PhD in materials joining/welding engineering from Ohio State.



Shelley Williams is a principal technologist with 16-years of experience at Sandia National Laboratories. She oversaw the laboratories and equipment that support the advancement of solder technology. Specializing in test design and execution for determining material properties, she worked with her team to evaluate

the performance and reliability of solder joints and soldered components to assess the impacts of aging and degradation over operational lifetimes. She supported Sandia mission work and cutting-edge research and development efforts with a broad portfolio of projects that advanced the state-of-the-art in solder technology. Currently, she oversees the laboratory and equipment that supports Sandia's Precision Cleaning Development Laboratory.



Paul T. Vianco received a Ph.D. degree in Materials Science from the University of Rochester (New York) in 1986. He joined Sandia National Laboratories, Albuquerque, New Mexico in 1987 and remained for 35 years until his retirement as a Senior Engineer. Paul has been involved in all aspects of soldering

technology, including alloy and process development as well as interface reactions and modeling to predict thermal mechanical fatigue. His studies also included numerous investigations into the physical and mechanical metallurgy of metal-to-ceramic, active braze joints. Vianco is a Fellow of the American Welding Society and ASM, International.